Cellular/Molecular

Differential Gating and Recruitment of P/Q-, N-, and R-Type Ca^{2+} Channels in Hippocampal Mossy Fiber Boutons

Liyi Li, Josef Bischofberger, and Peter Jonas
Physiologisches Institut der Universität Freiburg, Abteilung I, D-79104 Freiburg, Germany

Voltage-gated Ca^{2+} channels in presynaptic terminals initiate the Ca^{2+} inflow necessary for transmitter release. At a variety of synapses, multiple Ca^{2+} channel subtypes are involved in synaptic transmission and plasticity. However, it is unknown whether presynaptic Ca^{2+} channels differ in gating properties and whether they are differentially activated by action potentials or subthreshold voltage signals. We examined Ca^{2+} channels in hippocampal mossy fiber boutons (MFBs) by presynaptic recording, using the selective blockers ω-agatoxin IVa, ω-conotoxin GVIa, and SNX-482 to separate P/Q-, N-, and R-type components. Nonstationary fluctuation analysis combined with blocker application revealed a single MFB contained on average ~2000 channels, with 66% P/Q-, 26% N-, and 8% R-type channels. Whereas both P/Q-type and N-type Ca^{2+} channels showed high activation threshold and rapid activation and deactivation, R-type Ca^{2+} channels had a lower activation threshold and slower gating kinetics. To determine the efficacy of activation of different Ca^{2+} channel subtypes by physiologically relevant voltage waveforms, a six-state gating model reproducing the experimental observations was developed. Action potentials activated P/Q-type Ca^{2+} channels with high efficacy, whereas N- and R-type channels were activated less efficiently. Action potential broadening selectively recruited N- and R-type channels, leading to an equalization of the efficacy of channel activation. In contrast, subthreshold presynaptic events activated R-type channels more efficiently than P/Q- or N-type channels. In conclusion, single MFBs coexpress multiple types of Ca^{2+} channels, which are activated differentially by subthreshold and suprathreshold presynaptic voltage signals.

Key words: **mossy fiber boutons; presynaptic Ca^{2+} channels; P/Q-, N-, and R-type channels; hippocampus; channel gating; glutamatergic synapse**

Introduction

The mossy fiber–CA3 pyramidal neuron synapse is a key synapse in the trisynaptic circuitry of the hippocampus (Brown and Johnston, 1983; Henze et al., 2002; Nicoll and Schmitz, 2005; Bischofberger et al., 2006a). Although this synapse is widely used as a model to study presynaptic plasticity (Salin et al., 1996; Toth et al., 2000), the basic mechanisms of presynaptic Ca^{2+} signaling are incompletely understood.

Similar to other glutamatergic synapses, multiple types of Ca^{2+} channels contribute to synaptic transmission at hippocampal mossy fiber synapses (Castillo et al., 1994). The selective P/Q-type Ca^{2+} channel blocker ω-agatoxin IVa substantially reduces the amplitude of evoked EPSCs at both mossy fiber–pyramidal neuron and mossy fiber–interneuron synapses (Castillo et al., 1994; Pelkey et al., 2006). However, the selective N-type Ca^{2+} channel antagonist ω-conotoxin GVIa also inhibits synaptic transmission at mossy fiber synapses (Castillo et al., 1994; Pelkey et al., 2006). Finally, blockers of R-type Ca^{2+} channels inhibit mossy fiber long-term potentiation (LTP), although it has remained controversial whether these channels contribute to basal synaptic transmission (Gasparini et al., 2001; Breustedt et al., 2003; Dietrich et al., 2003). Recent imaging experiments suggested a large but highly variable (0–70%) contribution of R-type Ca^{2+} channels to action potential-evoked presynaptic Sr^{2+} transients in hippocampal mossy fiber boutons (MFBs) (Tokunaga et al., 2004; Miyazaki et al., 2005). Thus, multiple types of Ca^{2+} channels contribute to mossy fiber transmission, but their proportions at the level of single boutons and the conditions that lead to their activation have remained unclear.

Several recent studies suggest that electrical signaling in mossy fiber axons and boutons is more complex than previously thought (for review, see Bischofberger et al., 2006a) (see also Debanne, 2004). First, the duration of the presynaptic action potential is not constant, but shows broadening during repetitive stimulation (Geiger and Jonas, 2000). Second, activation of presynaptic $GABA_A$ receptors may exert an excitatory or inhibitory influence on MFBs (Ruiz et al., 2003; Price and Trussell, 2006). Finally, recent experiments revealed that subthreshold EPSPs propagate passively from the somatodendritic domain into the axon of granule cells (Alle and Geiger, 2006). Previous studies suggested that presynaptic Ca^{2+} channels in MFBs are activated efficiently by action potentials (Bischofberger et al., 2002). However, how the different subtypes of Ca^{2+} channels are activated by various voltage waveforms is unknown. This information is essential to understand

Received April 16, 2007; revised Sept. 17, 2007; accepted Oct. 8, 2007.

This work was supported by the Deutsche Forschungsgemeinschaft (SFB 505 and Leibniz program). We thank S. Becherer, M. Northemann, and K. Winterhalter for technical assistance.

Correspondence should be addressed to Dr. Peter Jonas, Physiologisches Institut, Universität Freiburg, Hermann-Herder-Strasse 7, D-79104 Freiburg, Germany. E-mail: peter.jonas@physiologie.uni-freiburg.de.

DOI:10.1523/JNEUROSCI.1709-07.2007

 0270-6474/07/2713420-10$15.00/0

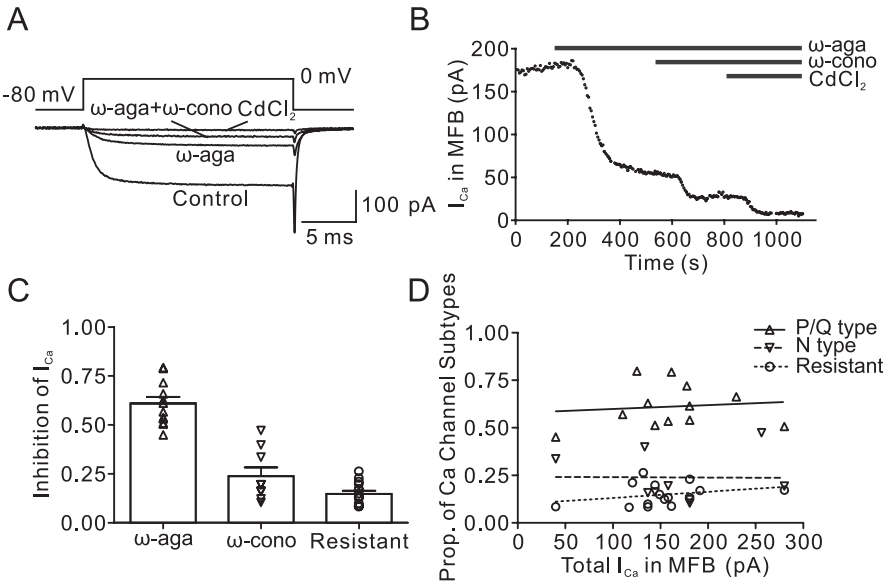

Figure 1. Pharmacological dissection reveals three components of the presynaptic Ca^{2+} current in hippocampal MFBs. ***A***, Presynaptic Ca^{2+} current evoked by a 20 ms pulse to 0 mV under control conditions, in the presence of 500 nM ω-agatoxin IVa (ω-aga), and after subsequent addition of 1 μM ω-conotoxin GVIa (ω-cono). The residual component was blocked by 200 μM Cd^{2+}, confirming that it was mediated by Ca^{2+} channels. ***B***, Plot of Ca^{2+} current amplitude against time during application of the toxins. The time of application of the blockers is indicated by the horizontal bars. Same bouton as shown in ***A***. ***C***, Summary bar graph illustrating the proportions of ω-agatoxin IVa-sensitive, ω-conotoxin GVIa-sensitive, and toxin-resistant component of the Ca^{2+} current. Symbols (triangles, inverted triangles, and circles) represent individual experiments, and bars represent mean ± SEM. Data are from 12, 9, and 15 boutons. ***D***, Plot of the proportions (Prop.) of the three components against the total Ca^{2+} current amplitude. Note the lack of correlation (Pearson's *r*, 0.11, −0.01, and 0.28; $p > 0.2$ in all cases).

the coupling between electrical signals and exocytosis or plasticity at hippocampal mossy fiber synapses.

To rigorously address these questions, we performed direct recordings from hippocampal MFBs (Bischofberger et al., 2006b). This approach allows us to accurately measure the presynaptic Ca^{2+} current under voltage-clamp conditions, as previously achieved at the squid giant synapse (Llinás et al., 1981; Augustine et al., 1985). Using presynaptic recordings, we addressed the following questions. First, do P/Q-, N-, and R-type Ca^{2+} channels coexist in a single presynaptic terminal? Second, does the gating differ between Ca^{2+} channel subtypes? Third, how efficiently are the different types of Ca^{2+} channels activated by presynaptic action potentials or subthreshold voltage signals?

Materials and Methods

Presynaptic recording. Transverse 300-μm-thick slices were cut from the hippocampus of 21- to 22-d-old Wistar rats, using a commercial (Dosaka DTK-1000, Kyoto, Japan) or a custom-built vibratome (Bischofberger et al., 2006b). The animals were killed by decapitation, in accordance with national and institutional guidelines. Slices were kept at 35°C for 30 min after slicing and then at room temperature. For the dissection and storage of slices, a solution containing 87 mM NaCl, 25 mM $NaHCO_3$, 10 mM glucose, 75 mM sucrose, 2.5 mM KCl, 1.25 mM NaH_2PO_4, 0.5 mM $CaCl_2$, and 7 mM $MgCl_2$ was used (equilibrated with 95% O_2/5% CO_2 gas mixture). For experiments, the slices were superfused with physiological saline containing 125 mM NaCl, 25 mM $NaHCO_3$, 25 mM glucose, 2.5 mM KCl, 1.25 mM NaH_2PO_4, 2 mM $CaCl_2$, and 1 mM $MgCl_2$ (95% O_2/5% CO_2).

Patch pipettes were pulled from borosilicate glass tubing (2.0 mm outer diameter, 0.6 mm inner diameter) and filled with a solution containing 145 mM CsCl, 2 mM $MgCl_2$, 2 mM Na_2ATP, 0.3 mM Na_2GTP, 5 mM Na_2-phosphocreatine, 10 mM EGTA, and 10 mM HEPES (pH adjusted to 7.3 with CsOH); pipette resistance was 7–9 MΩ. Mossy fiber boutons in stratum lucidum of the hippocampal CA3 region at a depth of ~30 μm from the slice surface were identified by their small diameter (3–5 μm), small capacitance (0.8–2 pF), and high input resistance (>1 GΩ) (Bischofberger et al., 2006b). Patch pipettes were positioned using a Kleindiek micromanipulator (Kleindiek Nanotechnik, Reutlingen, Germany). Currents were recorded with an Axopatch 700B amplifier (Molecular Devices, Sunnyvale, CA). Series resistance (≤50 MΩ) was compensated (60–85% correction, bandwidth 10 kHz). Data were filtered at 6 kHz (internal four-pole low-pass Bessel filter), and sampled at 50 kHz using a 1401 power interface (Cambridge Electronic Design, Cambridge, UK). For display purpose and nonstationary fluctuation analysis, data were passed through an additional 2.5 or 5 kHz low-pass digital filter. Pulse sequences were generated using FPulse (U. Fröbe, Physiologisches Institut der Universität Freiburg, Freiburg, Germany) running under Igor (version 5.01; WaveMetrics, Lake Oswego, OR) on a personal computer. Test pulses were applied at a frequency of 0.2 Hz. To isolate Ca^{2+} currents pharmacologically, 1 μM tetrodotoxin, 20 mM tetraethylammonium chloride (TEA), and 5 mM 4-aminopyridine (4-AP) were added to the bath solution. Capacitive and leakage currents were subtracted using the pipette capacitance compensation circuit of the amplifier and online digital P over −4 correction. Boutons were held at −80 mV throughout the experiment. Recordings were made at 23 ± 2°C.

ω-Conotoxin GVIa and ω-agatoxin IVa were from Bachem (Bubendorf, Switzerland), SNX-482 was from Peptides International (Louisville, KY), and nifedipine was from Sigma (St. Louis, MO). Other chemicals were obtained from Sigma, Merck (Darmstadt, Germany), Riedel-de Haën (Seelze, Germany), or Gerbu (Gaiberg, Germany). Peptide toxins were applied using a recirculation system with a peristaltic pump (Ismatec, Wertheim-Mondfeld, Germany). The total volume of the system was ~5 ml, and the solution was equilibrated with 95% O_2/5% CO_2. Bovine serum albumin (Sigma) was added at a concentration of 1 mg/ml to prevent adsorption of peptides to the surfaces of the system. In eight experiments, ω-conotoxin GVIa was applied before ω-agatoxin IVa, and in six other experiments, the order of application was reverse. Because the proportions of toxin-sensitive components of the Ca^{2+} current were similar, data were pooled. Because saturating concentrations of toxins and low-frequency stimulation were used, complications resulting from voltage-dependent toxin unblock were highly unlikely (Mintz et al., 1992; Forsythe et al., 1998).

Data analysis. The proportion of P/Q- and N- components in the presynaptic Ca^{2+} current was quantified by subtracting Ca^{2+} currents in the presence of ω-agatoxin IVa or ω-conotoxin GVIa from those before toxin application and measuring the amplitudes of the difference currents. Putative R-type channels were analyzed in the presence of ω-agatoxin IVa + ω-conotoxin GVIa. Throughout the paper, we refer to the residual current as R-type component, because (1) 500 nM SNX-482 blocked >50% of the residual current (Tottene et al., 2000; Metz et al., 2005), (2) 20 μM nifedipine had no effect on the residual current, excluding L-type channels, and (3) hyperpolarizing prepulses had no effect on the compound Ca^{2+} current, making T-type channels unlikely (see Results). For summary purpose, each proportion was normalized to the sum of all fractions (Fig. 1*C*). The time course of Ca^{2+} channel activation (0–5 ms after pulse onset) was fitted with an exponential function with delayed onset:

$$I(t) = I_0(1 - \exp[-(t - \delta)/\tau_a]) \text{ for } t \geq \delta \text{ and } 0 \text{ for } t < \delta, \quad (1)$$

where I_0 is the amplitude, τ_a is the activation time constant, and δ is the delay; the contribution of low-pass filtering (55 μs at 6 kHz) was sub-

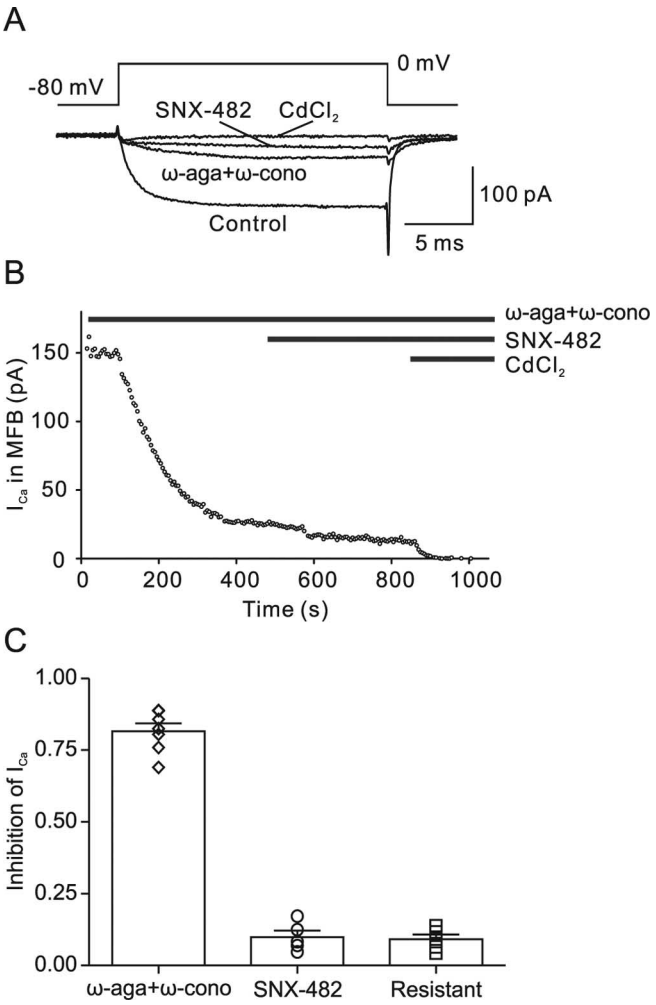

Figure 2. The agatoxin/conotoxin-resistant Ca^{2+} current component is primarily mediated by R-type channels. ***A***, Presynaptic Ca^{2+} current evoked by a 20 ms pulse to 0 mV under control conditions, in the presence of 500 nM ω-agatoxin IVa (ω-aga) + 1 μM ω-conotoxin GVIa (ω-cono), and after subsequent addition of 500 nM SNX-482. The residual component was completely blocked by 200 μM Cd^{2+}, confirming that it was mediated by Ca^{2+} channels. ***B***, Plot of Ca^{2+} current amplitude against time during application of the toxins. The time of application of the blockers is indicated by the horizontal bars. ***C***, Summary bar graph illustrating the proportions of ω-agatoxin IVa + ω-conotoxin GVIa-sensitive, SNX-482-sensitive, and toxin-resistant component of the Ca^{2+} current. Symbols (diamonds, circles, and squares) represent individual experiments, and bars represent mean ± SEM. Data are from seven, five, and five boutons.

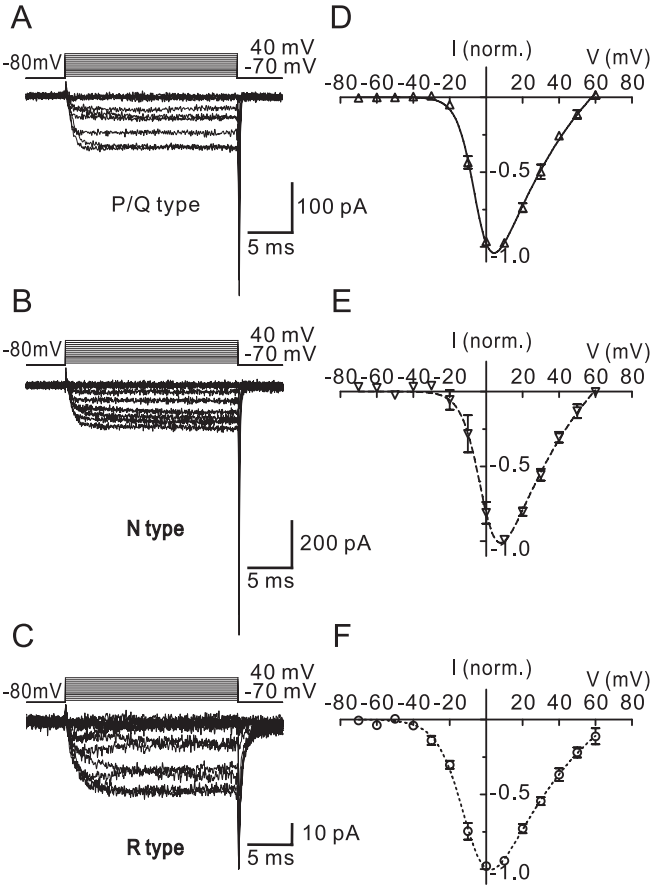

Figure 3. Voltage dependence of activation of P/Q-, N-, and R-type components of the presynaptic Ca^{2+} current. ***A–C***, Single traces of P/Q-type (***A***), N-type (***B***), and R-type (***C***) components of the presynaptic Ca^{2+} current obtained by pharmacological isolation and digital subtraction. Pulse protocol: holding potential −80 mV, test pulses to between −70 mV and +40 mV (10 mV increment), and step back to −80 mV. Traces in ***A–C*** are from three different boutons. ***D–F***, Average current–voltage relations of the three components. Current amplitudes were measured at the end of the 20 ms pulses and normalized (norm.) to the amplitude at 10 mV (***D***, ***E***) or 0 mV (***F***). Data points were fitted with Equation 2 (continuous, dashed, and dotted curves). Data are from six, five, and six boutons.

tracted. The time course of deactivation (0–3 ms after pulse end) was fitted with a single exponential. Voltage-clamp conditions were assessed from the 20–80% rise time of the tail current after a test pulse to 0 mV; the average value was 37.3 ± 2.0 μs in control conditions and 39.8 ± 2.6 μs in the presence of ω-conotoxin GVIa + ω-agatoxin IVa ($n = 19$; $p > 0.1$), indicating adequate voltage clamp for P/Q-, N-, and R-type components throughout the experiment. *I–V* relations were fitted with a product of a modified Goldman-Hodgkin-Katz equation and a Boltzmann term, giving the following function:

$$I(V) = PV([D - \exp(-V/C)]/[1 - \exp(V/C)]) \times [1 + \exp[(V_{mid} - V)/k]]^{-1}, \quad (2)$$

where P is an amplitude factor, C and D determine current rectification and reversal potential (Sala, 1991; Bischofberger et al., 2002), V_{mid} is the midpoint potential of the steady-state activation curve, and k is the corresponding slope factor.

For nonstationary fluctuation analysis (Sigworth, 1980), 15–138 Ca^{2+} current traces were analyzed. Ensemble mean versus time was determined by averaging all traces, whereas ensemble variance versus time was measured as the average of variances from overlapping pairs of traces, to minimize errors caused by run-down (Heinemann and Conti, 1992). Variance was plotted against mean for each time point. If the relation showed a parabolic shape, data were fitted with the following function:

$$\sigma^2(I) = iI - I^2/N + \sigma_0^2, \quad (3)$$

where σ^2 is variance, I is the mean current, i is the single-channel current, N is the number of channels in the patch, and σ_0^2 is the variance of the baseline noise (Sigworth, 1980). Alternatively, variance-mean data were fitted with the function $\sigma^2(I) = iI + \sigma_0^2$. For the estimation of maximal open probability and channel number, only experiments that could be fitted with the parabolic function were used (8/11 boutons under control conditions, 4/6 boutons in the presence of ω-conotoxin GVIa + ω-agatoxin IVa). This procedure may lead to a slight overestimation of maximal open probability and a corresponding underestimation of channel number.

Data analysis was performed using C-Stimfit (C. Schmidt-Hieber, Physiologisches Institut der Universität Freiburg, Freiburg, Germany), Graphpad Prism 4.0 (Graphpad, San Diego, CA), and Mathematica 4.1.2 or 5.0 (Wolfram Research, Champaign, IL). The values given in the text and the symbols and error bars in the figures indicate mean ± SEM. Traces shown in figures represent averages of 3–10 single sweeps, unless

Table 1. Gating and conductance properties of P/Q-, N-, and R-type Ca^{2+} channels in hippocampal MFBs

	V_{mid} (mV)	k (mV)	τ_{act} at 0 mV (ms)	τ_{deact} at −80 mV (ms)	i at 0 mV (pA)	Proportion of numbers of channels (%)
P/Q	−4.3 ± 0.7	4.7 ± 0.2	0.79 ± 0.05	0.09 ± 0.01	0.13 ± 0.02[a]	66
N	−2.6 ± 2.0	4.2 ± 0.5	0.93 ± 0.14	0.06 ± 0.01	0.13 ± 0.02[a]	26
R	−7.7 ± 2.1	6.7 ± 0.3	1.79 ± 0.28	0.55 ± 0.08	0.21 ± 0.05	8

[a]Values were obtained from analysis of the total Ca^{2+} current.

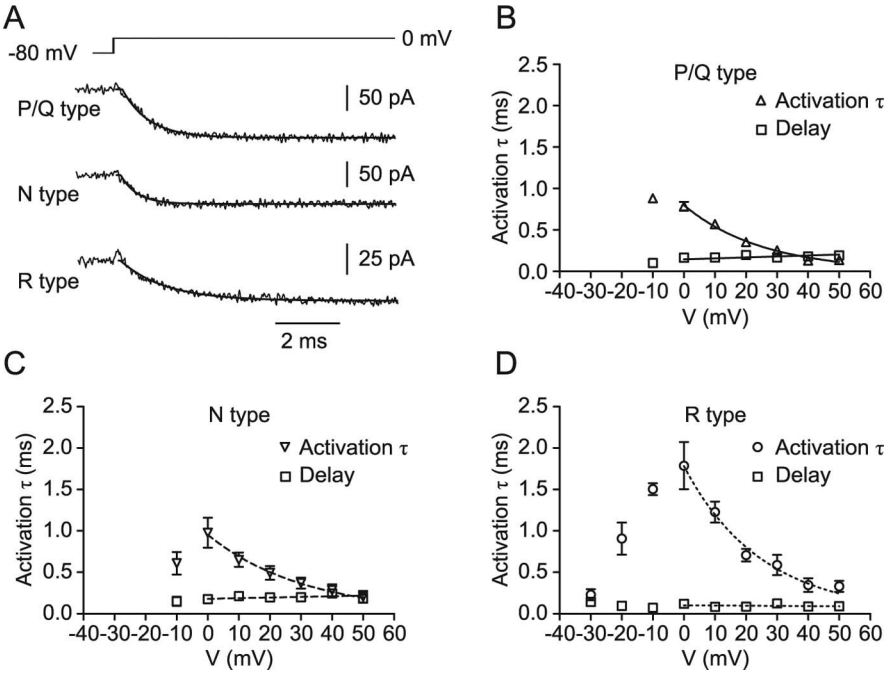

Figure 4. Activation kinetics of presynaptic P/Q-, N-, and R-type Ca^{2+} channels. ***A***, Traces of P/Q- (top trace), N- (center trace), and R- (bottom trace) type components of the presynaptic Ca^{2+} current obtained by pharmacological isolation and digital subtraction. Pulse protocol: holding potential −80 mV, test pulse to 0 mV. Traces were fitted with Equation 1 (continuous lines). ***B–D***, Activation time constant (inverted triangles, triangles, and circles) and delay (squares) for P/Q- (***B***), N- (***C***), and R- (***D***) type components. Time constant values for voltages ≥0 mV were fitted with exponential functions, and delay values were fitted by linear regression. Data are from five, five, and seven boutons.

specified differently. Membrane potentials are given without correction for liquid junction potentials. Differences were tested for statistical significance using a two-sided Wilcoxon signed-rank or a two-sided Mann–Whitney test at the significance level (p) indicated.

Modeling of Ca^{2+} channel gating. For each pharmacologically isolated Ca^{2+} current component, the total dataset comprised of steady-state activation curve, activation time constant and delay (−20 mV or −10 mV to +50 mV), deactivation time constant (−80 mV to −20 mV), and open probability at 0 mV was fitted with a multistate gating model that depicts the macroscopic current properties (Bischofberger et al., 2002; Engel and Jonas, 2005). The model consisted of five closed states and a single open state; all transitions except the last one preceding the open state were assumed to be voltage dependent. Because Ca^{2+} channels in MFBs showed only minimal inactivation during 20 ms test pulses to 0 mV (see Fig. 6*D*) or after 200–500 ms prepulses to potentials between −120 and −40 mV (not illustrated), inactivated states were not included in the model. Voltage-dependent forward and backward rates were calculated as follows:

$$\alpha_i(V) = \alpha_{i,0} \exp(V/k_i) \quad (4)$$

$$\beta_i(V) = \beta_{i,0} \exp(-V/k_i), \quad (5)$$

where $\alpha_{i,0}$ and $\beta_{i,0}$ are the forward and backward rates at 0 mV, k_i is the slope factor, and $i = 1 \ldots 4$. The sum of squares of differences between experimental observations and model predictions was minimized using a random walk algorithm and subsequently the FindMinimum function of Mathematica. Weight factors were set to the inverse of the maximum value in the dataset for kinetic data and to three times the inverse of this value for activation curve and open probability. The model is based on recordings at 23°C and thus depicts Ca^{2+} channel gating at this temperature.

To determine the efficacy of Ca^{2+} channel activation by physiological voltage waveforms, an action potential evoked by remote stimulation of the mossy fiber axon was used as a template. The action potential used had a duration at half-maximal amplitude of 0.54 ms [corresponding to the shortest in a sample of six propagated action potentials in our previous study (Bischofberger et al., 2002)]. To represent both variability of half-duration across MFBs and the effects of activity-dependent action potential broadening (Geiger and Jonas, 2000), longer action potentials were then generated from this template by scaling the repolarization phase in time. Subthreshold voltage signals were simulated as exponentially rising and decaying waveforms to approximate the shape of excitatory presynaptic potentials (EPreSPs) passively propagated to MFBs via the mossy fiber axon (Alle and Geiger, 2006).

Results

We characterized the Ca^{2+} channel subtypes expressed in hippocampal MFBs from 21- to 22-d-old rats. To isolate Ca^{2+} currents pharmacologically, 1 μM tetrodotoxin, 20 mM TEA, and 5 mM 4-AP were added to the bath solution. Figure 1*A* shows representative recordings of compound Ca^{2+} currents evoked by 20 ms test pulses to 0 mV obtained under these conditions. Presynaptic Ca^{2+} currents in MFBs showed activation properties similar to those reported previously (Bischofberger et al., 2002). In addition, Ca^{2+} currents showed only minimal steady-state inactivation tested with 100–500 ms prepulses (−120 mV to −40 mV; five boutons).

Coexistence of multiple Ca^{2+} channel subtypes in single mossy fiber boutons

To determine the contribution of different Ca^{2+} channel subtypes to the compound Ca^{2+} current, we applied the selective P/Q-type Ca^{2+} channel blocker ω-agatoxin IVa and the specific N-type channel blocker ω-conotoxin GVIa at saturating concentrations (Randall and Tsien, 1995; McDonough et al., 2002) (Fig. 1). 500 nM ω-agatoxin IVa blocked 61 ± 3% of the presynaptic Ca^{2+} current in hippocampal MFBs (12 boutons) (Fig. 1*B*,*C*). ω-Conotoxin GVIa (1 μM) blocked 24 ± 4% of the presynaptic Ca^{2+} current (nine boutons) (Fig. 1*B*,*C*). The remaining component, which had a relative amplitude of 15 ± 2%, was blocked by 200 μM Cd^{2+}, indicating that it was mediated by toxin-resistant Ca^{2+} channels. The three components were present in all boutons examined. Whereas the proportion of the P/Q-type component was relatively constant (with a coefficient of variation of 0.19), the proportion of both N- and R-type channels was

more variable (with coefficients of variation of 0.55 and 0.39). Regression analysis further revealed that the variability in the proportion of N- and R-type channels was independent of the Ca^{2+} current amplitude ($p > 0.2$ in all cases) (Fig. 1*D*).

The ω-agatoxin IVa-resistant, ω-conotoxin GVIa-resistant Ca^{2+} current component could be mediated by R-type, L-type, or (less likely) T-type Ca^{2+} channels (Catterall et al., 2005). We therefore tested the effects of the selective R-type channel blocker SNX-482 (Newcomb et al., 1998) (Fig. 2). After the application of a combination of 500 nM ω-agatoxin IVa and 1 μM ω-conotoxin GVIa, 500 nM SNX-482 was applied. On average, SNX-482 blocked 56 ± 3% of the ω-agatoxin IVa-resistant, ω-conotoxin GVIa-resistant Ca^{2+} current, corresponding to 10 ± 2% of the total Ca^{2+} current (five boutons). Because SNX-482 was previously shown to block only a subpopulation of R-type channels (Tottene et al., 2000; Metz et al., 2005), these results are consistent with the hypothesis that the toxin-resistant component is primarily mediated by R-type Ca^{2+} channels. To further test for the presence of L-type channels, we examined the effects of 20 μM nifedipine after coapplication of 500 nM ω-agatoxin IVa and 1 μM ω-conotoxin GVIa. However, application of 20 μM nifedipine had no detectable effect on the Ca^{2+} current amplitude (three boutons). To further test for the presence of T-type channels, we examined the effects of 100 ms prepulses to −120 mV on the Ca^{2+} current amplitude in the absence of toxins. However, hyperpolarizing prepulses increased the amplitude of the Ca^{2+} current by only 2.4 ± 1.9% of the total current (five boutons). Based on the effects of 500 nM SNX-482, which blocked >50% of the ω-agatoxin IVa-resistant, ω-conotoxin GVIa-resistant Ca^{2+} current, and the lack of effect of both nifedipine and prepulses, we conclude that the residual current is likely to be mediated by R-type channels.

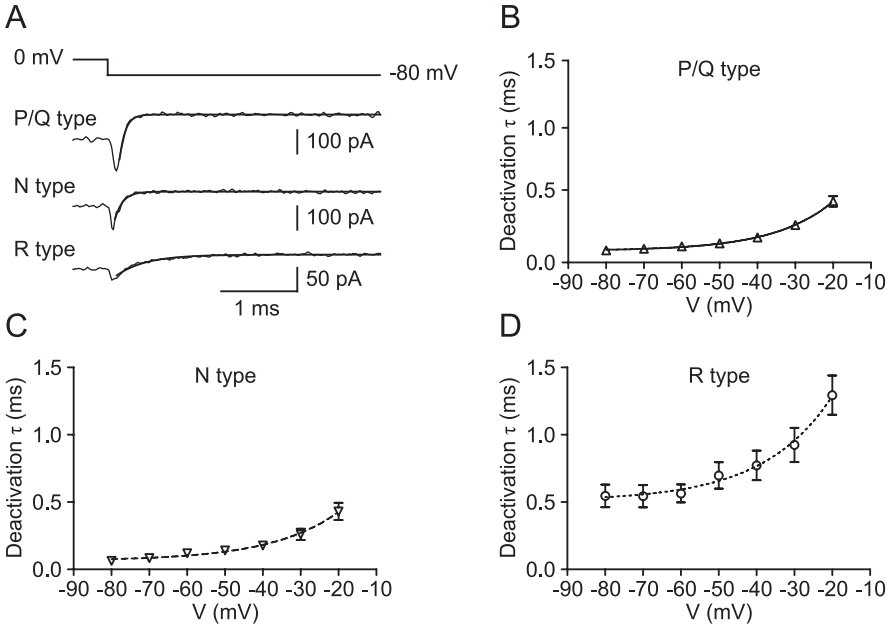

Figure 5. Deactivation kinetics of presynaptic P/Q-, N-, and R-type Ca^{2+} channels. ***A***, Traces of P/Q- (top trace), N- (center trace), and R- (bottom trace) type components of the presynaptic Ca^{2+} current obtained by pharmacological isolation and digital subtraction. Pulse protocol: holding potential −80 mV, 20 ms test pulse to 0 mV, and step back to −80 mV. Traces were fitted with an exponential function (continuous line). ***B–D***, Deactivation time constant for P/Q- (***B***), N- (***C***), and R- (***D***) type components. Data points were fitted with exponential functions. Data are from five, four, and seven boutons.

Differential gating of presynaptic P/Q-, N-, and R-type channels

To address the possible functional significance of the expression of P/Q-, N-, and R-type Ca^{2+} channels in MFBs, we characterized the voltage dependence of activation of the three types of channels (Fig. 3, Table 1). Test pulses (20 ms) to voltages between −70 and +60 mV were applied, and the corresponding Ca^{2+} currents were measured at the end of each pulse. P/Q- and N-type components were isolated by subtraction of current traces in the absence and presence of either ω-agatoxin IVa or ω-conotoxin GVIa, whereas R-type channels were characterized in the presence of a combination of the two blockers. Analysis of current–voltage relations of the three components revealed that the gating properties of the three components were significantly different. The activation threshold, quantified as the potential in which activation reached 10% of the maximal value, was −18.5 ± 1.0 mV for the P/Q-type component, −14.8 ± 3.4 mV for the N-type component, and −30.7 ± 1.8 mV for the R-type component ($p < 0.005$ for R-type versus P/Q- or N-type). Furthermore, the midpoint potential of the steady-state activation curve was −4.3 ± 0.7 mV for P/Q-type, −2.6 ± 2.0 mV for N-type, and −7.7 ± 2.1 mV for R-type channels, slightly, but not significantly, different between channels ($p > 0.05$). Finally, the slope factors of the activation curve were 4.7 ± 0.2 mV for P/Q-type, 4.2 ± 0.5 mV for N-type, and 6.7 ± 0.3 mV for R-type channels ($p < 0.01$ for R-type versus P/Q- or N-type). Thus, presynaptic R-type channels showed a lower activation threshold and a less steep voltage dependence of activation than P/Q- or N-type channels. P/Q-, N-, and R-type components showed only minimal inactivation during 20 ms pulses; the ratio of Ca^{2+} current at the end of a pulse to 0 mV (15–20 ms after onset) to that at the beginning (5–10 ms) was 1.05 ± 0.03, 1.06 ± 0.03, and 1.15 ± 0.07, respectively.

Next, we characterized the kinetics of activation and deactivation (Figs. 4, 5, Table 1). The activation time constant was measured from the onset of the Ca^{2+} current during the test pulses (Fig. 4*A*), and the deactivation time constant was determined using 20 ms test pulses to 0 mV followed by steps to voltages between −20 and −80 mV (Fig. 5*A*). Both the activation and deactivation time constants of P/Q- and N-type components were in the submillisecond range and were not significantly different from each other ($p > 0.1$). In contrast, the activation time constants of R-type channels were significantly slower between −10 and +10 mV ($p < 0.05$), and the deactivation time constants were substantially slower over the entire voltage range tested ($p < 0.05$). At −80 mV, the deactivation time constant for the R-type component was 0.55 ms, approximately six times slower than the deactivation of the P/Q-type component (0.09 ms). Thus, whereas the activation and deactivation kinetics of P/Q- and N-type channels were similar, activation and deactivation kinetics of R-type channels were markedly slower.

In summary, as depicted in Figure 6 and Table 1, P/Q-, N-, and R-type Ca^{2+} channels in MFBs differ in gating properties. Presynaptic R-type channels show a more negative activation threshold, less steep voltage dependence of activation, slower activation, and slower deactivation than P/Q- or N-type channels.

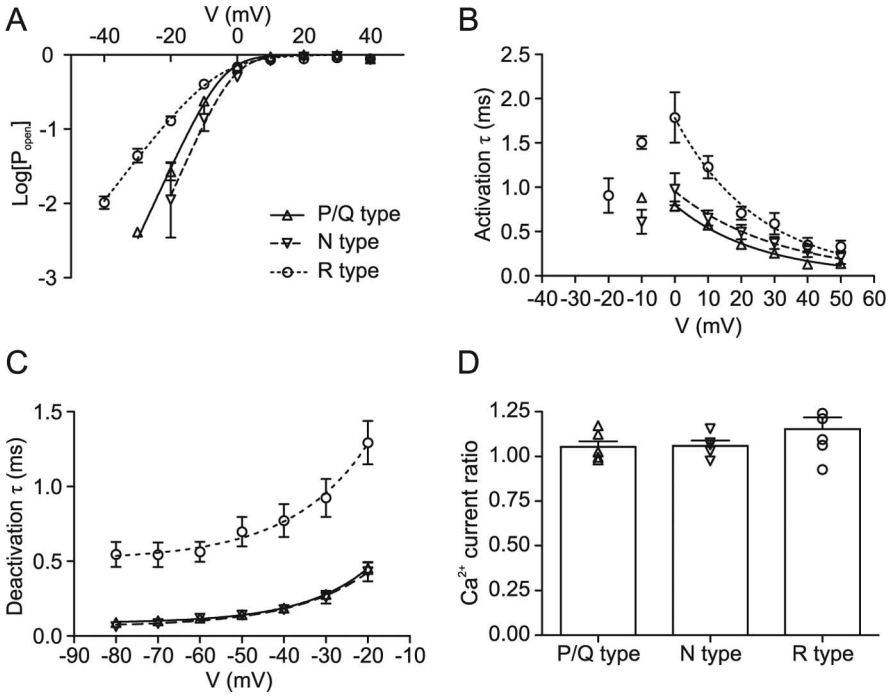

Figure 6. Summary of gating properties of presynaptic P/Q-, N-, and R-type channels. ***A***, Semilogarithmic plot of steady-state activation curve of P/Q- (triangles), N- (inverted triangles), and R- (circles) type components. The P_{open}–*V* relations were obtained from the *I*–*V* relations by dividing the current by the Goldman-Hodgkin-Katz factor in Equation 2, with values of *P*, *C*, and *D* taken from the fit of *I*–*V*s. Note that the activation curves of P/Q and N-type component are very similar, whereas the activation curve of the R-type component is less steep. ***B***, Plot of activation time constant against voltage. ***C***, Plot of deactivation time constant against voltage. Note that both activation and deactivation time constants are similar for P/Q- and N-type components, but slower for the R-type component. Data points in ***A*** were fitted with logarithmic Boltzmann functions, and data points in ***B*** and ***C*** were fitted by exponential functions (for voltages $\geq$0 mV in ***B***; continuous, dashed, and dotted curves). ***D***, Summary bar graph of ratio of Ca^{2+} current at the end (15–20 ms) and the beginning (5–10 ms) of 20 ms pulses to 0 mV for P/Q-, N-, and R-type components. In all cases, the ratio is close to 1, indicating the lack of inactivation.

Thus, fast, high voltage-activated and slow, low voltage-activated Ca^{2+} channels coexist in single hippocampal MFBs.

Single-channel conductance and channel numbers

We next determined the single-channel conductance (*i*), the maximal open probability, and the number of Ca^{2+} channels (*N*) present in a single MFB by nonstationary fluctuation analysis (Sigworth, 1980) (Fig. 7). Ca^{2+} currents were recorded using 20 ms test pulses to 0 mV. The ensemble variance was calculated from the fluctuation of currents, plotted against the ensemble mean, and fitted with a parabolic function (Eq. 3) (Fig. 7*B*). Under control conditions, the estimated single-channel current was 0.13 ± 0.02 pA, the maximal open probability of the channels at 0 mV was 0.74 ± 0.04, and the estimated number of channels was 2007 ± 455 (11, 8, and 8 boutons). In the presence of ω-agatoxin IVa + ω-conotoxin GVIa, which pharmacologically isolates R-type channels, the estimated single-channel current was 0.21 ± 0.05 pA, slightly, but not significantly, larger than in control conditions ($p > 0.1$; six boutons). Furthermore, the maximal open probability for the R-type component at 0 mV was 0.84 ± 0.04 ($p > 0.1$) and the estimated number of channels was 161 ± 41 (four boutons). Assuming that P/Q- and N-type channels have the same single-channel conductance, these results indicate that a large hippocampal MFB contains on average ~1300 P/Q-, ~500 N-, and ~160 R-type channels.

Differential activation of Ca^{2+} channel subtypes by presynaptic voltage waveforms

To determine the efficacy of Ca^{2+} channel activation by subthreshold and suprathreshold presynaptic voltage signals, we developed kinetic models of the gating of P/Q-, N-, and R-type Ca^{2+} channels (Hille, 2001) (Fig. 8, Table 2). For each pharmacologically isolated Ca^{2+} channel subtype, we fitted the steady-state activation curve (Fig. 8*A*,*C*,*E*), activation time constant and delay, deactivation time constant (Fig. 8*B*,*D*,*F*), and open probability at 0 mV with a gating model that consisted of five closed states and a single open state; all transitions except the last one preceding the open state were assumed to be voltage dependent. The four voltage-dependent transitions were necessary to account for the delay in activation. The final, voltage-independent step was required to describe the maximal open probability of Ca^{2+} channels and the relatively slow and voltage-independent deactivation of the R-type channels (Fig. 8*F*). As shown in Figure 8, the gating of all three types of channels is closely reproduced by the model. However, for R-type channels, the forward rates from C4 to O and the backward rates from O to C4 were smaller than those of P/Q- and N-type channels. This was necessary to account for the relatively slow and voltage-independent deactivation kinetics of R-type channels.

Using the experimentally constrained models of P/Q-, N-, and R-type channel gating, we examined the activation of the three types of channels by physiological voltage waveforms (Fig. 9). We first tested whether the models accurately predicted the Ca^{2+} current evoked by a short propagated action potential (duration at half-maximal amplitude 0.54 ms) in MFBs. Figure 9*A* shows a Ca^{2+} current activated by a short action potential in an MFB under control conditions and in the presence of ω-agatoxin IVa + ω-conotoxin GVIa, isolating the R-type component. Figure 9*B* shows the corresponding predictions of the models, which accurately reproduced the experimentally recorded action potential-evoked Ca^{2+} currents. For all three components, the peak of the Ca^{2+} current occurred during the repolarization phase of the action potential, as reported previously for the compound Ca^{2+} current in MFBs at both 23°C (Bischofberger et al., 2002) and 34°C (Geiger and Jonas, 2000) (but see Sabatini and Regehr, 1999).

We then used the models to determine the efficacy of Ca^{2+} channel activation for the three types of presynaptic Ca^{2+} channels. The short action potential activated P/Q-, N-, and R-type channels with peak efficacies of 0.65, 0.50, and 0.49, respectively (Fig. 9*C*). Thus, short action potentials activated P/Q-type channels more efficiently than N- or R-type channels. In contrast, a broadened action potential in which the repolarization phase was scaled by a factor of three (Geiger and Jonas, 2000) activated P/Q-, N-, and R-type channels with efficacies of 0.90, 0.82, and 0.76 (Fig. 9*D*). Thus, broader action potentials activated the three types of channels with more comparable efficacy. When the du-

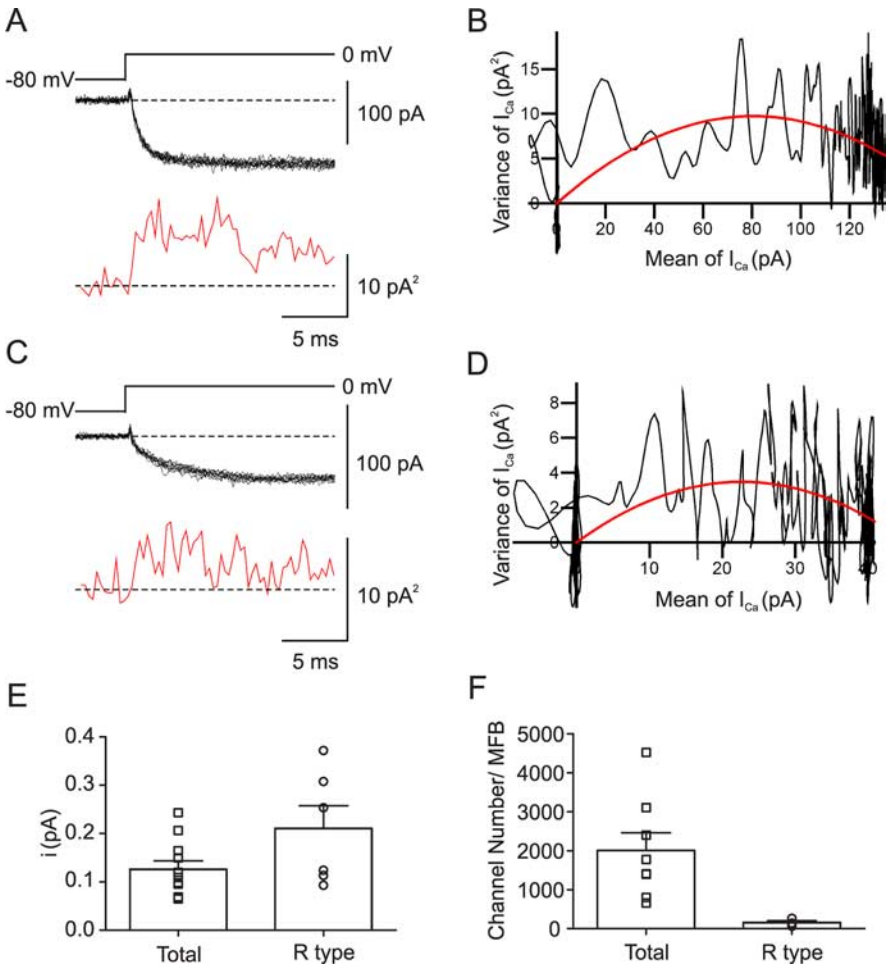

Figure 7. Single-channel conductance and number of Ca^{2+} channels in hippocampal MFBs. ***A***, ***C***, 10 consecutive traces of Ca^{2+} currents evoked by steps from −80 to 0 mV (black traces) and mean variance calculated from 15 adjacent points (red trace) under control conditions (***A***) and in the presence of 500 nM ω-agatoxin IVa + 1 μM ω-conotoxin GVIa (***C***). ***B***, ***D***, Plot of variance against mean under control conditions (***B***) and in the presence of 500 nM ω-agatoxin IVa + 1 μM ω-conotoxin GVIa (***D***). Data were fitted by Equation 3 (red curve). Baseline noise was subtracted. The single-channel current and the total number of channels were 0.24 pA and 664 under control conditions (***B***) and 0.31 pA and 148 in the presence of ω-agatoxin IVa + ω-conotoxin GVIa (***D***). Data in ***A*** and ***B*** were obtained from a different bouton from those in ***C*** and ***D***. ***E***, Summary bar graph of single-channel current (*i*) in control conditions and in the presence of ω-agatoxin IVa + ω-conotoxin GVIa. ***F***, Summary bar graph of number of channels per MFB in control conditions and in the presence of ω-agatoxin IVa + ω-conotoxin GVIa.

ration of the action potential repolarization phase was systematically increased by scaling the repolarization phase of the short action potential, the efficacy of P/Q-type channel activation increased only moderately, whereas the efficacy of N- and R-type channel activation increased substantially (Fig. 9*E*). Finally, EPreSPs to −50 mV activate R-type channels with an efficacy of 1×10^{-3}, approximately five times more efficiently than P/Q- and N-type channels (2×10^{-4}) (Fig. 9*F*). Furthermore, a series of five EPreSPs to −50 mV will generate a total Ca^{2+} inflow via R-type channels comparable with that induced by a single action potential (71%). Thus, despite the low number of R-type channels, their activation by subthreshold stimuli is expected to have a large impact on slow Ca^{2+}-dependent processes in hippocampal MFBs.

Discussion

We characterized the abundance and kinetics of Ca^{2+} channel subtypes at a hippocampal presynaptic terminal by whole-cell voltage-clamp recording. Three major findings are reported. First, we find that P/Q-, N-, and R-type Ca^{2+} channels coexpressed in single MFBs differ in gating properties. Whereas presynaptic P/Q- and N-type Ca^{2+} channels show high activation threshold and fast gating, presynaptic R-type channels show a lower activation threshold and slower gating. Second, our results show that R-type channels are preferentially activated by broadened action potentials and subthreshold presynaptic voltage signals, which readily explains their selective involvement in mossy fiber plasticity (Breustedt et al., 2003; Dietrich et al., 2003). Finally, using nonstationary fluctuation analysis, we obtained the first quantitative estimates of single-channel conductance, absolute open probability, and numbers of Ca^{2+} channels per bouton. Our results are critically important for understanding how action potentials and subthreshold presynaptic voltage signals trigger and modulate transmitter release from hippocampal MFBs.

Channel types, conductance properties, and channel numbers

Previous imaging data with Sr^{2+} as a charge carrier suggested a large contribution of R-type Ca^{2+} channels to action potential-induced divalent inflow in MFBs (Tokunaga et al., 2004; Miyazaki et al., 2005). Whereas ω-agatoxin IVa and ω-conotoxin GVIa reduced the amplitude of the Sr^{2+} transients by 33 and 20%, the remaining fraction (47%) was resistant to these blockers but was partially inhibited by SNX-482 (Tokunaga et al., 2004; Miyazaki et al., 2005). In contrast, our direct recording from MFBs revealed that the P/Q-type Ca^{2+} current component (61%) dominates over both N- and R-type components (24 and 15% of the total Ca^{2+} current). These findings appear to be more consistent with the observation that transmitter release at mossy fiber synapses is primarily mediated by P/Q-type Ca^{2+} channels (Castillo et al., 1994; Pelkey et al., 2006).

We further obtained quantitative estimates of both single-channel conductances and channel numbers for the three types of Ca^{2+} channels by nonstationary fluctuation analysis. With Ca^{2+} as a charge carrier at physiological concentrations, the single-channel current at 0 mV was 0.13 pA for the total channel population and 0.21 pA for R-type channels, corresponding to chord conductances of 2.2 and 3.5 pS (assuming a reversal potential of +60 mV). Fluctuation analysis also allowed us to determine the total (i.e., open + closed) number of Ca^{2+} channels in a hippocampal MFB. On average, a single large bouton contained ~1300 P/Q-, ~500 N-, and ~160 R-type channels. In relative terms, 66% of Ca^{2+} channels are P/Q-type, 26% N-type, and 8% R-type. As MFBs, on average, have 29.7 active zones at an age comparable with that used in the present study (four fully reconstructed MFBs at P28) (Rollenhagen et al., 2007) (see also Chicurel and Harris, 1992; Acsády et al., 1998), these total channel numbers correspond to 44 P/Q-type channels, 17 N-type chan-

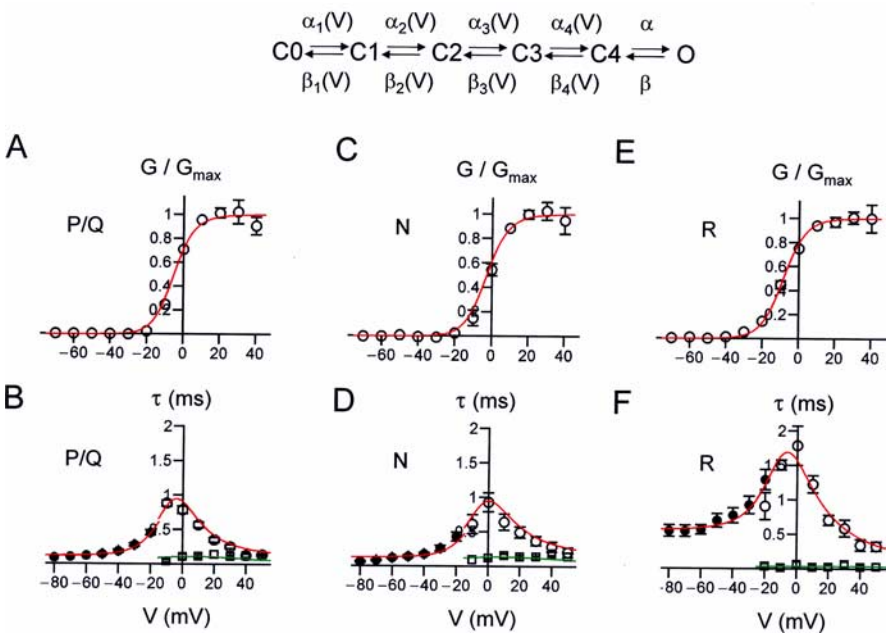

Figure 8. Gating models for presynaptic P/Q-, N-, and R-type channels. ***A***, ***B***, Modeling of voltage dependence of steady-state activation (***A***, open circles), activation time constant (***B***, open circles), delay (***B***, open squares), and deactivation time constant (***B***, filled circles) for presynaptic P/Q-type channels. ***C–F***, Similar analysis for N-type (***C***, ***D***) and R-type channels (***E***, ***F***). The scheme on top indicates the structure of the kinetic model. The predictions of the models are indicated by red (activation curve, activation time constant, deactivation time constant) and green curves (delays). For model parameters, see Table 2.

Table 2. Gating models of P/Q-, N-, and R-type Ca^{2+} channels in hippocampal MFBs

$\alpha_{i,0}$ (ms^{-1})	$\beta_{i,0}$ (ms^{-1})	k_i (mV)
P/Q-type channel model		
$\alpha_{1,0} = 5.89$	$\beta_{1,0} = 14.99$	$k_1 = 62.61$
$\alpha_{2,0} = 9.21$	$\beta_{2,0} = 6.63$	$k_2 = 33.92$
$\alpha_{3,0} = 5.20$	$\beta_{3,0} = 132.80$	$k_3 = 135.08$
$\alpha_{4,0} = 1823.18$	$\beta_{4,0} = 248.58$	$k_4 = 20.86$
$\alpha = 247.71$	$\beta = 8.28$	
N-type channel model		
$\alpha_{1,0} = 4.29$	$\beta_{1,0} = 5.23$	$k_1 = 68.75$
$\alpha_{2,0} = 5.24$	$\beta_{2,0} = 6.63$	$k_2 = 39.53$
$\alpha_{3,0} = 4.98$	$\beta_{3,0} = 73.89$	$k_3 = 281.62$
$\alpha_{4,0} = 772.63$	$\beta_{4,0} = 692.18$	$k_4 = 18.46$
$\alpha = 615.01$	$\beta = 7.68$	
R-type channel model		
$\alpha_{1,0} = 9911.36^a$	$\beta_{1,0} = 0.62^a$	$k_1 = 67.75$
$\alpha_{2,0} = 4.88$	$\beta_{2,0} = 21.91$	$k_2 = 50.94$
$\alpha_{3,0} = 4.00$	$\beta_{3,0} = 51.30$	$k_3 = 173.29$
$\alpha_{4,0} = 256.41$	$\beta_{4,0} = 116.97$	$k_4 = 16.92$
$\alpha = 228.83$	$\beta = 1.78$	

[a]For this step, $\alpha_{1,0}$ is large, and $\beta_{1,0}$ is small. Thus, omitting C0 and the associated transitions would only make minimal differences.

nels, and 5 R-type channels per active zone. It will be interesting to compare these numbers with the number of presynaptic particles in MFB freeze-fracture material, which are thought to be primarily Ca^{2+} channels (Pumplin et al., 1981).

Differential gating of presynaptic Ca^{2+} channel subtypes

Understanding the coupling between presynaptic action potentials and exocytosis at cortical glutamatergic synapses requires quantitative analysis of the gating properties of presynaptic Ca^{2+} channels. Previously we analyzed the kinetic properties of the compound Ca^{2+} current in MFBs (Bischofberger et al., 2002). However, as the new data show, the presynaptic Ca^{2+} current is carried by a functionally heterogeneous population of Ca^{2+} channel subtypes. The properties of these subtypes are difficult to infer from the analysis of recombinant channels, because the subunit composition of the presynaptic Ca^{2+} channels including accessory subunits and other Ca^{2+} channel interaction partners is not precisely known. These factors may substantially affect Ca^{2+} channel gating (for review, see Arikkath and Campbell, 2003). For example, association of Ca^{2+} channel α subunits with $\alpha 2/\delta$ subunits shifts the activation curve in the hyperpolarizing direction (Felix et al., 1997), whereas association with syntaxin was reported to enhance inactivation (Bezprozvanny et al., 1995; Hurley et al., 2004). Thus, direct analysis of gating of native Ca^{2+} channels in presynaptic terminals is required.

The electrotonic structure of the mossy fiber terminals and the presynaptic location of the Ca^{2+} channels allowed us to study their gating properties under almost ideal voltage-clamp conditions. The rise time of the Ca^{2+} tail currents, which are almost instantaneous, indicates that the Ca^{2+} channels are located in mossy fiber terminals rather than adjacent axons. For the MFB, this means that the speed of voltage clamp is limited by the kinetics of the charging of the bouton, which occurs with a time constant $\tau = R_s \times C_{MFB} \approx 15\ M\Omega \times 2\ pF = 30\ \mu s$, where R_s is the uncompensated series resistance and C_{MFB} is the bouton capacitance (Geiger and Jonas, 2000; Hallermann et al., 2003) (see Materials and Methods). Thus, direct recording from hippocampal MFBs allows us to study the gating of identified Ca^{2+} channel subtypes with unique temporal resolution.

Under these near-optimal voltage-clamp conditions, we found subtle differences between the gating of P/Q- and N-type channels, but markedly different functional properties of R-type channels. Presynaptic N-type channels showed a slightly, but not significantly, more positive midpoint potential of activation curve, but almost identical activation and deactivation kinetics than P/Q-type channels. These findings are consistent with the slight differences between native and recombinant P/Q- and N-type channels reported previously (Wheeler et al., 1996; Colecraft et al., 2000). In contrast, presynaptic R-type channels in MFBs showed a markedly lower activation threshold and a shallower steady-state activation curve than P/Q- or N-type channels, consistent with previous data for recombinant channels (Bourinet et al., 1996). Furthermore, presynaptic R-type channels showed slower activation and deactivation kinetics than P/Q- or N-type channels. Thus, presynaptic Ca^{2+} channel types differ in gating properties, suggesting differential involvement in synaptic transmission.

The present study also suggests several differences between the gating of Ca^{2+} channels in the hippocampal MFB and the calyx of Held. First, the midpoint potential of activation of all Ca^{2+} current components in MFBs is more positive than that of the total Ca^{2+} current in the calyx (−23 mV) (Borst and Sakmann, 1998). Second, in MFBs the activation threshold of R-type channels is lower than that of P/Q- and N-type channels, whereas in the calyx the voltage-dependencies of the Ca^{2+} channel components are

more similar (Wu et al., 1999). Finally, in MFBs the coexistence of P/Q-, N-, and R-type channels is maintained at relatively mature developmental stages. In contrast, in the calyx of Held, N- and R-type channels coexist with P/Q-type channels until postnatal day 10 and are downregulated later in development (Iwasaki et al., 2000). These findings suggest that the Ca^{2+} channel properties are highly specialized in the MFB, but more homogeneous in the calyx, especially in mature synapses.

Differential recruitment of Ca^{2+} channels by presynaptic voltage waveforms

Several recent studies suggest that signaling in mossy fiber axons and MFBs is highly complex (for review, see Bischofberger et al., 2006a) (see also Debanne, 2004). First, the duration of the presynaptic action potential is not constant, but shows broadening during repetitive stimulation (Geiger and Jonas, 2000). Action potential broadening has been also reported in neocortical axons (Shu et al., 2006), suggesting a general feature of cortical axons and presynaptic terminals. Second, recent experiments revealed that subthreshold synaptic events propagate passively from the somatodendritic domain of granule cells to MFBs (Alle and Geiger, 2006). This may suggest that information in the mossy fiber system is coded by both action potential ("digital") and subthreshold ("analog") signals. Both spike duration coding and analog coding may enrich the computational repertoire of mossy fiber axons (Alle and Geiger, 2006; Bischofberger et al., 2006a).

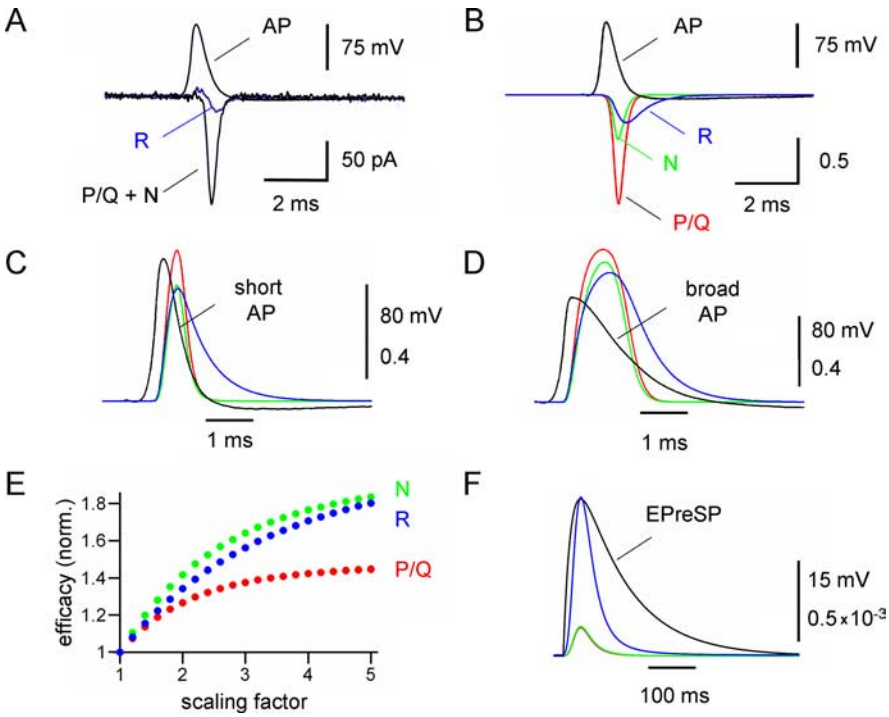

Figure 9. Efficacy of Ca^{2+} channel activation by natural presynaptic voltage waveforms. ***A***, Contribution of P/Q-, N-, and R-type channels to the Ca^{2+} current evoked by a short action potential (AP) in a whole-cell recorded MFB. Top traces, action potentials used as voltage-clamp commands. Bottom traces, Ca^{2+} currents evoked by the stimulus waveform under control conditions and in the presence of 500 nM ω-agatoxin IVa + 1 μM ω-conotoxin GVIa. ***B***, Simulated Ca^{2+} currents carried by P/Q-type channels (red curve), N-type channels (green curve), and R-type channels (blue curve) during a short action potential. ***C***, ***D***, Open probability of P/Q-type channels (red curves), N-type channels (green curves), and R-type channels (blue curves), during short (***C***) and broadened (***D***) action potential waveforms (black curves). Broadened action potentials were generated by scaling of the repolarization phase in time by a factor of three. ***E***, Plot of peak efficacy of Ca^{2+} channel activation against the scaling factor, normalized (norm.) to the peak efficacy obtained with the unscaled action potential. For P/Q-type Ca^{2+} channels (red circles), the efficacy increased only moderately, whereas for N- (green circles) and R-type Ca^{2+} channels (blue circles) the efficacy increased substantially as the action potential was prolonged. ***F***, Open probability of P/Q-type channels (red curves), N-type channels (green curves), and R-type channels (blue curves), during a subthreshold depolarization with slow exponential rise and decay (rise time constant 20 ms, decay time constant 100 ms), approximating the shape of previously recorded EPreSPs in MFBs (Alle and Geiger, 2006).

How do these electrical events activate the different types of presynaptic Ca^{2+} channels in MFBs (Sabatini and Regehr, 1999)? Whereas short action potentials activate P/Q-type channels with higher efficacy than N-type or R-type channels, broadened action potentials activate the different channel types with more similar efficacy. Hence, action potential broadening will lead to selective recruitment of N- and R-type Ca^{2+} channels. Furthermore, subthreshold voltage signals will selectively activate R-type channels. For a subthreshold EPreSP reaching a peak amplitude of −50 mV, the open probability of R-type channels is approximately five times larger than that of P/Q- and N-type channels. In the calyx of Held, a minimal Ca^{2+} inflow through P/Q-type Ca^{2+} channels activated by subthreshold stimuli induces a significant increase in synaptic strength (Awatramani et al., 2005). In the MFB, the larger Ca^{2+} inflow through R-type Ca^{2+} channels is expected to increase synaptic strength even more profoundly, thus contributing to posttetanic potentiation or LTP at mossy fiber synapses (Salin et al., 1996; Breustedt et al., 2003; Dietrich et al., 2003). Because granule cells in the behaving animal fire with low frequency (Jung and McNaughton, 1993), but receive rhythmic excitatory synaptic input during theta oscillations (Ylinen et al., 1995), Ca^{2+} inflow through R-type channels activated by subthreshold events may be relevant for mossy fiber plasticity *in vivo*.

References

Acsády L, Kamondi A, Sík A, Freund T, Buzsáki G (1998) GABAergic cells are the major postsynaptic targets of mossy fibers in the rat hippocampus. J Neurosci 18:3386–3403.

Alle H, Geiger JRP (2006) Combined analog and action potential coding in hippocampal mossy fibers. Science 311:1290–1293.

Arikkath J, Campbell KP (2003) Auxiliary subunits: essential components of the voltage-gated calcium channel complex. Curr Opin Neurobiol 13:298–307.

Augustine GJ, Charlton MP, Smith SJ (1985) Calcium entry into voltage-clamped presynaptic terminals of squid. J Physiol (Lond) 367:143–162.

Awatramani GB, Price GD, Trussell LO (2005) Modulation of transmitter release by presynaptic resting potential and background calcium levels. Neuron 48:109–121.

Bezprozvanny I, Scheller RH, Tsien RW (1995) Functional impact of syntaxin on gating of N-type and Q-type calcium channels. Nature 378:623–626.

Bischofberger J, Geiger JRP, Jonas P (2002) Timing and efficacy of Ca^{2+} channel activation in hippocampal mossy fiber boutons. J Neurosci 22:10593–10602.

Bischofberger J, Engel D, Frotscher M, Jonas P (2006a) Timing and efficacy of transmitter release at mossy fiber synapses in the hippocampal network. Pflügers Arch 453:361–372.

Bischofberger J, Engel D, Li L, Geiger JRP, Jonas P (2006b) Patch-clamp recording from mossy fiber terminals in hippocampal slices. Nature Protocols 1:2075–2081.

Borst JGG, Sakmann B (1998) Calcium current during a single action potential in a large presynaptic terminal of the rat brainstem. J Physiol (Lond) 506:143–157.

Bourinet E, Zamponi GW, Stea A, Soong TW, Lewis BA, Jones LP, Yue DT, Snutch TP (1996) The α_{1E} calcium channel exhibits permeation properties similar to low-voltage-activated calcium channels. J Neurosci 16:4983–4993.

Breustedt J, Vogt KE, Miller RJ, Nicoll RA, Schmitz D (2003) α_{1E}-containing Ca^{2+} channels are involved in synaptic plasticity. Proc Natl Acad Sci USA 100:12450–12455.

Brown TH, Johnston D (1983) Voltage-clamp analysis of mossy fiber synaptic input to hippocampal neurons. J Neurophysiol 50:487–507.

Castillo PE, Weisskopf MG, Nicoll RA (1994) The role of Ca^{2+} channels in hippocampal mossy fiber synaptic transmission and long-term potentiation. Neuron 12:261–269.

Catterall WA, Perez-Reyes E, Snutch TP, Striessnig J (2005) International Union of Pharmacology. XLVIII. Nomenclature and structure-function relationships of voltage-gated calcium channels. Pharmacol Rev 57:411–425.

Chicurel ME, Harris KM (1992) Three-dimensional analysis of the structure and composition of CA3 branched dendritic spines and their synaptic relationships with mossy fiber boutons in the rat hippocampus. J Comp Neurol 325:169–182.

Colecraft HM, Brody DL, Yue DT (2000) G-protein inhibition of N- and P/Q-type calcium channels: distinctive elementary mechanisms and their functional impact. J Neurosci 21:1137–1147.

Debanne D (2004) Information processing in the axon. Nat Rev Neurosci 5:304–316.

Dietrich D, Kirschstein T, Kukley M, Pereverzev A, von der Brelie C, Schneider T, Beck H (2003) Functional specialization of presynaptic $Ca_v2.3$ Ca^{2+} channels. Neuron 39:483–496.

Engel D, Jonas P (2005) Presynaptic action potential amplification by voltage-gated Na^+ channels in hippocampal mossy fiber boutons. Neuron 45:405–417.

Felix R, Gurnett CA, De Waard M, Campbell KP (1997) Dissection of functional domains of the voltage-dependent Ca^{2+} channel $\alpha_2\delta$ subunit. J Neurosci 17:6884–6891.

Forsythe ID, Tsujimoto T, Barnes-Davies M, Cuttle MF, Takahashi T (1998) Inactivation of presynaptic calcium current contributes to synaptic depression at a fast central synapse. Neuron 20:797–807.

Gasparini S, Kasyanov AM, Pietrobon D, Voronin LL, Cherubini E (2001) Presynaptic R-type calcium channels contribute to fast excitatory synaptic transmission in the rat hippocampus. J Neurosci 21:8715–8721.

Geiger JRP, Jonas P (2000) Dynamic control of presynaptic Ca^{2+} inflow by fast- inactivating K^+ channels in hippocampal mossy fiber boutons. Neuron 28:927–939.

Hallermann S, Pawlu C, Jonas P, Heckmann M (2003) A large pool of releasable vesicles in a cortical glutamatergic synapse. Proc Natl Acad Sci USA 100:8975–8980.

Heinemann SH, Conti F (1992) Nonstationary noise analysis and application to patch clamp recordings. Methods Enzymol 207:131–148.

Henze DA, Wittner L, Buzsáki G (2002) Single granule cells reliably discharge targets in the hippocampal CA3 network *in vivo*. Nat Neurosci 5:790–795.

Hille B (2001) Ionic channels of excitable membranes (3rd edition). Sunderland, MA: Sinauer.

Hurley JH, Cahill AL, Wang M, Fox AP (2004) Syntaxin 1A regulation of weakly inactivating N-type Ca^{2+} channels. J Physiol (Lond) 560:351–363.

Iwasaki S, Momiyama A, Uchitel OD, Takahashi T (2000) Developmental changes in calcium channel types mediating central synaptic transmission. J Neurosci 20:59–65.

Jung MW, McNaughton BL (1993) Spatial selectivity of unit activity in the hippocampal granular layer. Hippocampus 3:165–182.

Llinás R, Steinberg IZ, Walton K (1981) Presynaptic calcium currents in squid giant synapse. Biophys J 33:289–322.

McDonough SI, Boland LM, Mintz IM, Bean BP (2002) Interactions among toxins that inhibit N-type and P-type calcium channels. J Gen Physiol 119:313–328.

Metz AE, Jarsky T, Martina M, Spruston N (2005) R-type calcium channels contribute to afterdepolarization and bursting in hippocampal CA1 pyramidal neurons. J Neurosci 25:5763–5773.

Mintz IM, Adams ME, Bean BP (1992) P-type calcium channels in rat central and peripheral neurons. Neuron 9:85–95.

Miyazaki K, Ishizuka T, Yawo H (2005) Synapse-to-synapse variation of calcium channel subtype contributions in large mossy fiber terminals of mouse hippocampus. Neuroscience 136:1003–1014.

Newcomb R, Szoke B, Palma A, Wang G, Chen X, Hopkins W, Cong R, Miller J, Urge L, Tarczy-Hornoch K, Loo JA, Dooley DJ, Nadasdi L, Tsien RW, Lemos J, Miljanich G (1998) Selective peptide antagonist of the class E calcium channel from the venom of the tarantula *Hysterocrates gigas*. Biochemistry 37:15353–15362.

Nicoll RA, Schmitz D (2005) Synaptic plasticity at hippocampal mossy fibre synapses. Nat Rev Neurosci 6:863–876.

Pelkey KA, Topolnik L, Lacaille JC, McBain CJ (2006) Compartmentalized Ca^{2+} channel regulation at divergent mossy-fiber release sites underlies target cell-dependent plasticity. Neuron 52:497–510.

Price GD, Trussell LO (2006) Estimate of the chloride concentration in a central glutamatergic terminal: a gramicidin perforated-patch study on the calyx of Held. J Neurosci 26:11432–11436.

Pumplin DW, Reese TS, Llinás R (1981) Are the presynaptic membrane particles the calcium channels? Proc Natl Acad Sci USA 78:7210–7213.

Randall A, Tsien RW (1995) Pharmacological dissection of multiple types of Ca^{2+} channel currents in rat cerebellar granule neurons. J Neurosci 15:2995–3012.

Rollenhagen A, Sätzler K, Patricia Rodríguez E, Jonas P, Frotscher M, Lübke JHR (2007) Structural determinants of transmission at large hippocampal mossy fiber synapses. J Neurosci 27:10434–10444.

Ruiz A, Fabian-Fine R, Scott R, Walker MC, Rusakov DA, Kullmann DM (2003) $GABA_A$ receptors at hippocampal mossy fibers. Neuron 39:961–973.

Sabatini BL, Regehr WG (1999) Timing of synaptic transmission. Annu Rev Physiol 61:521–542.

Sala F (1991) Activation kinetics of calcium currents in bullfrog sympathetic neurones. J Physiol (Lond) 437:221–238.

Salin PA, Scanziani M, Malenka RC, Nicoll RA (1996) Distinct short-term plasticity at two excitatory synapses in the hippocampus. Proc Natl Acad Sci USA 93:13304–13309.

Shu Y, Hasenstaub A, Duque A, Yu Y, McCormick DA (2006) Modulation of intracortical synaptic potentials by presynaptic somatic membrane potential. Nature 441:761–765.

Sigworth FJ (1980) The variance of sodium current fluctuations at the node of Ranvier. J Physiol (Lond) 307:97–129.

Tokunaga T, Miyazaki K, Koseki M, Mobarakeh JI, Ishizuka T, Yawo H (2004) Pharmacological dissection of calcium channel subtype-related components of strontium inflow in large mossy fiber boutons of mouse hippocampus. Hippocampus 14:570–585.

Toth K, Suares G, Lawrence JJ, Philips-Tansey E, McBain CJ (2000) Differential mechanisms of transmission at three types of mossy fiber synapse. J Neurosci 20:8279–8289.

Tottene A, Volsen S, Pietrobon D (2000) α_{1E} subunits form the pore of three cerebellar R-type calcium channels with different pharmacological and permeation properties. J Neurosci 20:171–178.

Wheeler DB, Randall A, Tsien RW (1996) Changes in action potential duration alter reliance of excitatory synaptic transmission on multiple types of Ca^{2+} channels in rat hippocampus. J Neurosci 16:2226–2237.

Wu LG, Borst JGG, Sakmann B (1999) R-type Ca^{2+} currents evoke transmitter release at a rat central synapse. Proc Natl Acad Sci USA 95:4720–4725.

Ylinen A, Soltész I, Bragin A, Penttonen M, Sik A, Buzsáki G (1995) Intracellular correlates of hippocampal theta rhythm in identified pyramidal cells, granule cells, and basket cells. Hippocampus 5:78–90.